Journal of Colloid and Interface Science 696 (2025) 137725

Contents lists available at ScienceDirect

Journal of Colloid And Interface Science

journal homepage: www.elsevier.com/locate/jcis

Regular Article

Exploring the onset of the nonlinear start-up response of wormlike micelles through rheology and rheo-microscopy: Banding & scission

Ilaria Cusano [a], Afshin Azarpour [b], Luca Laugeni [a], Simona Russo Spena [a], Pedro Rodriguez Gonzalez [c], Dganit Danino [c,d], Nino Grizzuti [a], Giuliano Zanchetta [b], Rossana Pasquino [a,*]

[a] Department of Chemical, Materials and Production Engineering, University of Naples Federico II, P.le Tecchio, 80, Naples, 80125, Italy
[b] Department of Medical Biotechnology and Translational Medicine, Università degli Studi di Milano, V. F.lli Cervi, 93, Segrate (MI), 20054, Italy
[c] Cryo-EM and Self-Assembly Laboratory, Guangdong-Technion Israel Institute of Technology, Shantou, China
[d] Cryo-EM Laboratory of Soft Matter, Faculty of Biotechnology and Food Engineering, Technion-Israel Institute of Technology, Haifa, Israel

GRAPHICAL ABSTRACT

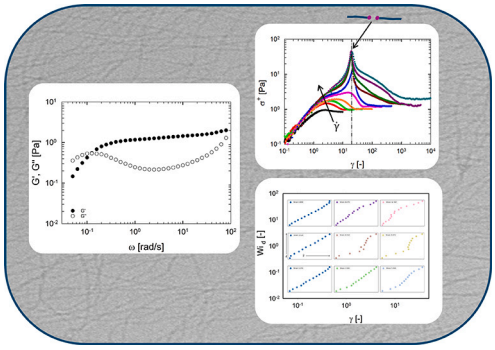

ABSTRACT

This study aims to offer new insights and perspective into the linear and nonlinear rheology of a wormlike micellar solution containing a well known surfactant, cetylpyridinium chloride, and a binding salt, diclofenac sodium. The wormlike micelles (WLMs) mesoscopic lengths were evaluated through rheology. The micrometer long micelles, disclosed also with cryogenic -Electron Microscopy (cryo-EM), were subjected to start-up flow experiments, both with a rotational rheometer and with a linear strain controlled shear cell coupled with a microscope. In the nonlinear regime, two Weissenberg numbers can be defined, one related to the terminal relaxation time, Wi_d, and one connected to the breaking and reforming time, Wi_b. When $Wi_d < 1$, the measured stress response is monotonically increasing up to a steady state value, and the resulting velocity profile is stable. When $Wi_d > 1$, the WLMs behave as polymer chains in fast flows, aligning and stretching in the flow direction. When a characteristic shear rate is reached, WLMs show a very pronounced strain hardening behavior, with a stress peak typical of an elastic chain response. When $Wi_b >> 1$, the stress peak appears at the same strain units above a characteristic shear rate value. A sudden stress decrease manifests after the peak, suggesting a breakage phenomenon. The strain at which the stress peak appears permits the evaluation of the WLMs scission energy. The reconstruction of the velocity profiles along the gap of the sample, thanks to a home made rheo-optical device, and the complete flow curve of the system, built with the help of a bio-printer used as a capillary rheometer, suggest that a shear banding phenomenon appears when Wi_d is roughly equal to one. No direct connection between banding and scission has been experimentally found.

* Corresponding author.
E-mail address: r.pasquino@unina.it (R. Pasquino).

https://doi.org/10.1016/j.jcis.2025.137725
Received 17 March 2025; Received in revised form 26 April 2025; Accepted 27 April 2025
Available online 8 May 2025

1. Introduction

Surfactants, a class of self-assembling amphiphilic molecules, possess intriguing properties that are the focus of research and industrial applications [1,2]. In solution, these molecules tend to rearrange into ordered colloidal structures, called micelles, which limit the exposure of their hydrophobic tails to water. Such structures may undergo conformational changes in response to temperature [3], pH [4], or the presence of additives [5]. In particular, the addition of a penetrating salt, characterized by having at least one aromatic ring, induces a spherical-to-wormlike micellar transition [6,7]. Such wormlike micelles (WLMs) display most intriguing viscoelastic properties, analogous to those observed in polymers. The key distinction between polymers and WLMs lies in the nature of the bonds that are created between the molecules. Unlike the stronger covalent bonds that connect polymer chains, micellar bonds are physical [8] and subject to continuous breakage and reformation at the microstructural length scale, hence the epithet of living polymers. Increasing the salt concentration in solution can induce further conformational transitions, leading to entangled [9] or branched micelles [10], or even a shift to vesicles and lamellar phases [11]. By performing linear rheology tests, information can be deduced on the micellar self-assemblies, and on their characteristic relaxation times [12]. Mesoscopic WLMs length scales can be evaluated from viscoelastic spectra using established scaling laws [13].

In general, the relaxation dynamics of WLMs are well described by the Cates model [14], which is based on two specific relaxation phenomena: a reptation process, which characterizes the sliding of the worm within a tubular constraint created by the surrounding WLMs, and a breaking and reforming time, which considers micelles rearrangement. The two characteristic times can be evaluated from linear viscoelasticity tests according to the equations:

$$\tau_b = \frac{1}{\omega_{min}} \tag{1}$$

$$\tau_r = \frac{\tau_d^2}{\tau_b} \tag{2}$$

where τ_b and τ_r are the breaking and reptation times, respectively; ω_{min} is the angular frequency which corresponds to the minimum of the loss modulus, G''_{min}, and τ_d is the disengagement time, evaluated as the inverse of the crossover frequency at which the viscoelastic moduli cross in a dynamic test. The average entanglement number, Z, can also be expressed as the ratio between $G'_{\min}$ and $G''_{\min}$. $G'_{\min}$ is the value of the storage modulus at the angular frequency at which $G''_{\min}$ is detected. Additionally, the Cates model enables to estimate the characteristic lengths of the wormlike micelles, including the entanglement length, l_e, and the contour length L_c, which are the typical distance between two network nodes and an underestimation of the total length of the WLMs, respectively [14,15]. Unfortunately, it is only possible to estimate these lengths once the persistence length, l_p, which correlates with the stiffness of the micelle, has been determined. Indeed, it is difficult to achieve a broad range in frequency exclusively through rheology. At very high frequencies, where bending modes of Kuhn segments dominate, another crossover frequency, ω_0, can be detected [16]. If measurable, the persistence length can be estimated through [17]

$$\omega_0 = \frac{k_B T}{8\eta_s {l_p}^3} \tag{3}$$

where k_B is the Boltzmann constant, T is the experimental temperature, η_s is the solvent viscosity. As such, the experimental tests typically combine standard rheology with specialized devices or optical techniques [17–19].

Following Cates, several authors have focused their efforts on further elaborating the description of WLMs relaxation dynamics [20–23]. In this context, Tan et al. [24] developed new expressions for the linear viscoelastic properties as a function of l_e and L_c by correlating the predictions of the mesoscopic pointer algorithm [23,25] with the microscopic slip-spring model [26]:

$$G_0 = \frac{\alpha^3}{3+\alpha^3} \cdot 9.75 \frac{k_B T}{\alpha^{1.8} l_p^3} + \frac{3}{3+\alpha^3} \cdot \frac{28}{5\pi} \frac{\varphi k_B T}{d^2 \alpha l_p} \tag{4}$$

$$\frac{G'_{\min}}{G''_{\min}} = 0.317 \left(\frac{L_c}{l_e} \right)^{0.82} \tag{5}$$

where G_0 is the plateau modulus, α is a so-called semi-flexibility factor (defined as the ratio between l_e and l_p), φ is the micelles volume fraction, d is the micelle diameter. In this scenario, cryo-EM is an effective technique to couple with WLMs rheology, as it allows direct visualization of the micelles and their morphology [27–29].

In our recent work in very dilute wormlike micellar solutions, the whole relaxation spectrum was covered by linear rheology [13]. More specifically, we have found that diluted micellar solutions of cetylpyridinium chloride (CPyCl), a widely studied ionic surfactant, and diclofenac sodium (Diclo), a non-steroidal anti-inflammatory drug, are characterized by exceptionally long and rigid WLMs, enabling the measurement of all characteristic parameters without the need for additional techniques beyond linear rheology.

Moreover, the properties of the CPyCl-Diclo systems also make them a non-trivial test bench for the investigation of the rich nonlinear behavior of WLMs when subjected to strong flows, a scenario that is frequently encountered in industrial contexts. The Weissemberg number, defined as $Wi_d = \tau_d \dot{\gamma}$, where $\dot{\gamma}$ is the applied shear rate, is the threshold between linear and nonlinear regime. When Wi_d exceeds 1, the system is subjected to a strong force field and WLMs' flow can exhibit complex features: shear thinning, which represents the result of the alignment and stretching of the micelles along the flow direction [10,30,31]; shear banding, which is a flow instability resulting in the micellar solution splitting into bands of different concentrations and shear rates across the gap [3,32,33]; and strain hardening, which is the sudden increase in the shear stress growth coefficient [34].

More specifically, WLMs can show non-equilibrium phase coexistence arising along the gradient direction between an isotropic solution and an aligned (paranematic) band with lower viscosity than the quiescent phase [35–37]. These bands result from mechanical instability, producing two branches (shear bands), one at low and the other at high shear rates. Band sizes typically follow the lever rule. In a simple shear-banding scenario, the fluid is divided into just two clear regions separated by a thin, steady interface of very small width.

The phenomenon of strain hardening in micellar solutions was first identified in 1988 by Shikata et al. [30], who conducted nonlinear step strain and step rate experiments on a system of cetyltrimethylammonium bromide (CTAB) and sodium salicylate (NaSal). Later studies by Brown et al. [38] investigated this phenomenon in more detail in the same systems, identifying strain hardening only when the strain overcame 3.5. In 1994, Proud'homme and Warr [39] observed strain hardening during extensional tests, and suggested a possible correlation between this phenomenon and WLMs scission, proposing that the observed decrease in stress growth coefficient post-hardening was due to the breakage of WLMs. Rothstein [40] later corroborated this hypothesis by performing extensional tests on the CTAB/NaSal systems using a filament stretching rheometer, determining a scission energy close to $4k_BT$, consistent with predictions made by Turner and Cates in 1992 [41]. Since then, various studies have further explored strain hardening, providing evidence of its correlation with the WLMs finite extensibility. Indeed, it is well-established that the WLMs network can store energy up to a certain maximum deformation, after which scission can eventually take place [34,42–46].

In most complex fluids, nonlinear bulk rheological response often corresponds to local alignment and structural rearrangements occurring at the microscale. These can be triggered and probed through active microrheology approaches which provide access to local mechanical properties by applying an external force to an embedded microparti-

cle [47,48]. However, such methods miss the coupling of structural rearrangements with macroscopic deformations, which requires the application of a technique capable of nano-, micro- or mesoscale resolution to the sample, while it is subjected to bulk stress/strain application. For example, rheo-SANS (Small Angle Neutron Scattering) gives access to non-affine local flow fields of WLMs during large amplitude oscillations [49], and rheo-microscopy can provide critical information on deformation profiles [50], degree of alignment [51], or local rearrangements [52].

In the present work, an investigation is conducted into a distinctive sample, based on CPyCl and Diclo, which displays the entire relaxation time spectra within the experimental frequency window in linear rheology, and a distinguished nonlinear response in start-up flow. Its flow curve is built in a wide range of shear rates, by combining classical rotational rheometry with a printer used as a capillary rheometer. The evaluation of the theoretical scission energy and its actual correlation with the energy cumulated by the shear work during a steady test are discussed. To gain insight into the origin of the peculiar rheological behavior displayed by CPyCl-Diclo, we run parallel rheo-microscopy experiments of shear start-up, estimating the time-dependent deformation profiles across the gap during the accumulation of strain, combined with cryo-EM analysis of the micelles. We discuss a non-trivial correlation between WLMs banding and scission.

2. Materials and methods

2.1. Materials

The sample, 16.7 mM CPyCl 11.0 mM Diclo, was prepared by dissolving both chemicals (available as powders from Sigma-Aldrich) in double-distilled water, according to the methodology detailed in [13].

2.2. Rheology

Linear viscoelasticity tests were conducted on a stress-controlled rheometer DHR-2, from TA Instruments, equipped with 40 mm-diameter sandblasted parallel plates. A Peltier cell was employed for temperature control and a solvent trap used to prevent evaporation. Once the linear viscoelasticity regime was identified, dynamic frequency sweep tests (DFST) were conducted in the angular frequencies range of $[100; 0.05] rad/s$, with a strain of 10% and a constant temperature of 25 °C.

Nonlinear rheology tests were performed with a strain-controlled ARES rheometer (TA instruments, USA), equipped with a 50 mm-diameter cone-plate geometry. The transient behavior of the micellar solution was investigated through step-rate tests at a series of fixed shear rates, under room temperature (kept at 25 °C). For each investigated shear rate, a fresh sample was loaded.

Since nonlinear shear measurements are affected by instabilities as the sample is subjected to strong flow [53], a 3D bioprinter (BIOX Cellink, Göteborg, Sweden), operated as a capillary rheometer, was used to achieve very high shear rates. The test procedure was conducted according to the protocol outlined in [54]. The experiments were carried out at 25 °C, using a nozzle of 33 mm in length and 0.413 mm in diameter, within the pressure range $[3; 30]$ kPa. Given the high lenght-to-diameter ratio, the flow can be assumed to be fully developed. Shear stress and viscosity as a function of shear rate were obtained by applying the standard relations for capillary rheometry [55] when a known pressure drop is applied.

Extensional rheology tests were conducted using a home-made experimental setup, which was developed based on the *Ambient DoS rheometer* described in [56]. A syringe pump was connected to a capillary with an external diameter equal to 1.8 mm, and used at a fixed flow rate of 22 µl/min. Filament formation was achieved by adopting the *stationary drop* [57] approach. This involved the gradual elevation of the bottom plate, until contact with the drop was established, at a distance of approximately 1.5 mm from the nozzle. A high-speed camera (iX Cameras, i-SPEED 203) with a frame rate of 50 frames per second (fps) was then used to capture the resulting images. Finally, a MATLAB routine was built to process the data.

2.3. Rheo-microscopy

The sample was loaded between the two parallel plates of a linear strain-controlled shear-cell (RheOptiCAD, CAD Instruments, France) [58], modified to enable bright-field imaging and coupled to a Nikon Eclipse Ti-S inverted microscope. Although the linear geometry limits the total attainable strain, it guarantees a uniform strain at the confining surfaces, while providing optical access to the sample. The glass slides were sandblasted to minimize slip of the sample, except for a small central window kept clear for optical access. We can impose continuous displacement of one plate, while keeping the opposite plate fixed, or simultaneous motion of both plates to achieve higher total strain and shear rate. Polystyrene microparticles (diameter 1.04 µm, Microparticles GmbH) were dispersed in the sample at a volume fraction of about $5 \cdot 10^{-4}$ to optically reconstruct the flow field in the sample, without affecting its rheological properties. The gap was kept constant at 300 µm, well above any relevant length scale of the system. The focus was adjusted at different heights across the gap. The vertical resolution is about 20 micrometers, as obtained by keeping the condenser (LWD, NA = 0.52) diaphragm open, thus reducing the coherence of illumination and minimizing the depth-of-focus and the thickness of the layer in which tracers are visible [50]. Measurements were performed at a constant temperature of 25 °C. Images were acquired using a 10× objective and a CMOS camera (Ximea xiC MC031MG-SY) with a rectangular region of interest (ROI) of 617 µm × 183 µm, or a high-speed sCMOS camera (Teledyne Prime BSI Express) with a ROI of 1163 µm × 144 µm. The frame rate was adjusted between 10 Hz and 557 Hz, depending on the imposed shear rate. This configuration enabled high-resolution reconstruction of the trajectories of hundreds of tracer particles within a single experiment over sufficiently long time intervals. Image processing was performed using a custom Python code to identify potential heterogeneities within the imaging planes and extract the average tracer velocity for each height and time interval.

2.4. Cryo-EM

Cryo-EM samples were prepared at 25 °C using a Vitrobot Mark 4 in a water vapor-saturated environment. A 5 µL droplet was applied to a Quantifoil R1.2/1.3 copper grid. Excess solution was removed via blotting with filter paper on rotating foam pads under controlled conditions. After a 10–15 second relaxation period, the grid was plunged into liquid ethane, vitrified, and stored in liquid nitrogen. The vitrified samples were analyzed with a 200 kV Glacios TEM using a Falcon 4 direct detector at low-dose conditions, with nominal magnifications ranging between 73k and 190k [59].

3. Results and discussion

3.1. Rheological response

Fig. 1 reports the linear viscoelastic moduli, along with the complex viscosity, as a function of the angular frequency. The sample shows a strong viscoelastic behavior, typical of a wormlike micellar network. The micelles relax on a very long time scale, with a total relaxation time of the order of seconds (the inverse of the crossover at low frequencies, τ_d), and present an elastic plateau, G_0, spanning more than two decades in frequency. As already shown in a recent work [13], the very low surfactant concentration allows to cover the entire relaxation spectrum. The inverse of the crossover at high frequencies, τ_0, has been extrapolated from the linear viscoelastic response and allows a direct estimation of

Table 1
Characteristic viscoelastic parameters and extrapolated lengths.

G_0 [Pa]	τ_d [s]	τ_b [s]	τ_r [s]	τ_0 [s]	Z [−]	l_p [nm]	l_e [nm]	L_c [nm]
1.26	7.9	0.4	156	0.008	6	160	530	19200

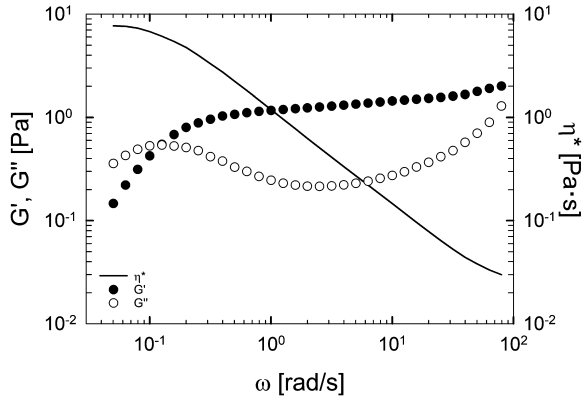

Fig. 1. Linear viscoelastic moduli of the investigated surfactant solution (left axis) and corresponding complex viscosity (right axis).

the wormlike micelles persistence length (Equation (3)). The reptation time τ_r of the micelles can be easily evaluated through Equation (2). The relatively low zero-frequency viscosity (roughly 10 Pa·s) and the high relaxation time suggest the presence of very long, loosely entangled ($Z = 6$, evaluated as stated in the Introduction) wormlike micelles, with a contour length roughly close to 20 micrometers, obtained by using Equation (4) and Equation (5). The complete set of viscoelastic parameters and approximate characteristic lengths are summarized in Table 1. A direct visualization of the micelles through cryo-EM is reported in Fig. 2, confirming the morphology inferred by the linear viscoelasticity. Micelles indeed appear very long (no chain ends can be distinguished in the images) and entangled.

Fig. 3 shows the results of the capillary-thinning experiment on the micellar solution. In Fig. 3 a), six snapshots of the filament are reported, acquired during the test. From these images, the temporal evolution of the filament thinning can be tracked [60,61]. The transition from the viscocapillary region, VC, distinguished by an hourglass shape, to the elastocapillary region, EC, characterized by a column shape of the filament, is then followed by the occurrence of the pinch-off in the region of finite extensibility, FE. Fig. 3 b) displays the filament diameter as a function of time. The three capillarity regions can also be identified. In the initial time interval, the VC Newtonian behavior barely appears, characterized by a linear decrease of the diameter with time. Then, in the central portion of the graph, which extends until approximately 60 seconds, the behavior departs from Newtonian, with D_{min} exhibiting an exponential reduction over time (EC behavior). In the final section, the FE phase, the diameter exhibits again a linear decrease over time, indicating the return to Newtonian behavior, at enhanced extensional rate, until the filament breaks. A regression procedure was conducted in the EC region to evaluate the constant extensional rate, $\dot{\varepsilon}$, and the extensional relaxation time, λ_E, in accordance with the equations:

$$\dot{\varepsilon}(t) = -\left[\frac{2}{D(t)}\right]\left(\frac{\mathrm{d}D(t)}{\mathrm{d}t}\right) \tag{6}$$

$$D \sim \exp\left(-\frac{t}{3\lambda}\right) \tag{7}$$

The procedure returned two values, the stretching rate and the extensional relaxation time equal to $0.03s^{-1}$ and $25.5s$, respectively. The latter is roughly 3 times the shear relaxation time, τ_d (Table 1), a factor already observed for other micellar solutions [62,56].

Start-up experiments were performed in a wide range of shear rates/Weissenberg (Wi) numbers, as reported in Fig. 4a. In the legend, two Wi numbers are reported at the same value of the shear rate: the first one is obtained by multiplying the shear rate by τ_d and the other by τ_b. We will refer to Wi_d and Wi_b, respectively. At low shear rates (when both Wi_s are lower than 1), the stress growth coefficient monotonically increases up to a steady state. When Wi_d overcomes unity, and Wi_b is still lower than 1, viscosity shows a peak, before reaching the steady state value. In this regime, micelles behave like polymer chains, aligning, stretching and tumbling in the flow direction, as already discussed elsewhere [63]. When $Wi_d > 1$ and Wi_b is roughly close to one, a pronounced strain hardening appears, followed by a well defined maximum and a subsequent sudden viscosity drop, which brings to a "noisy" steady state value. In this shear rate range, the micellar system cannot renew itself with the well-known breaking/reptation-fluctuation mechanism described in the literature: the system remains frozen in a complex micellar structure, and displays a rubber-like response.

The same data are shown in Fig. 4b, where the stress growth function is now reported as a function of strain, evaluated as the product of the experimental time and the imposed shear rate. It is apparent that the data for the fastest flows superimpose to form a single master curve. This feature strongly suggests that at these rates the material behaves as a permanent rubber. Similar responses have been discussed in Inoue et al. [34] and Pasquino et al. [46]. The upturn at $\gamma = 8$ is clearly due to the finite extensibility of the network strands, whereas the peak at $\gamma_{max} = 20$ is due to a major collapse of the network structure. A similar trend is reported for the first normal stress growth function in Supplementary Information (SI). To rationalize the characteristic times for the onset of this behavior, we have reviewed a few systems in literature, with similar start-up responses [34,46]. The results are reported in SI. It appears clear that all the surfactant systems show hardening when a critical shear rate is reached, usually placed in between $1/\tau_d$ and $1/\tau_b$.

3.1.1. WLMs scission

Start-up measurements suggest that the micellar network experiences an abrupt relaxation at roughly 20 strain units. The latter could be considered as a critical value, above which the micellar network breaks *en masse*, under the applied shear work. The breakage probably involves only a part, although major, of the WLMs, if one thinks of a (narrow) lengths distribution. Consequently, after network collapse, not all chains are broken, with the smallest ones probably still intact. The stress, following its peak, is insufficient to cause further chain scission, and the distribution of micelle lengths requires additional time to fully attain a steady state.

Although the picture may seem quite quirky, we can compare the scission energy exerted by the experimental shear work with the predicted scission energy for a single chain, from existing theoretical models [12,64]. The experimental scission energy corresponding to the observed drop at γ_{max} can be evaluated through elasticity theory [65] as:

$$E_{sciss,exp} = \frac{1}{2}k\gamma_{max}^2 L_c^2 = \frac{1}{2}\frac{A}{L_c}G_0\gamma_{max}^2 L_c^2 = \frac{1}{2}AG_0\gamma_{max}^2 L_c \tag{8}$$

with k the "usual" elastic constant, A the cross section of the WLMs, the diameter being equal to twice the hydrophobic chain length of the surfactant molecule ($A = 1.76 \cdot 10^{-17}\ m^2$). The estimated $E_{sciss,exp}$ is $0.85\ 10^{-19}$ Joule.

We can compare this value with the theoretical scission energy, required to create two new chain ends from a single test chain, by pulling them in opposite direction [64]:

$$E_{\mathrm{sciss}} \sim 2k_B T \ln\left(\frac{N_{\mathrm{agg}}}{\varphi^{0.5}}\right) \tag{9}$$

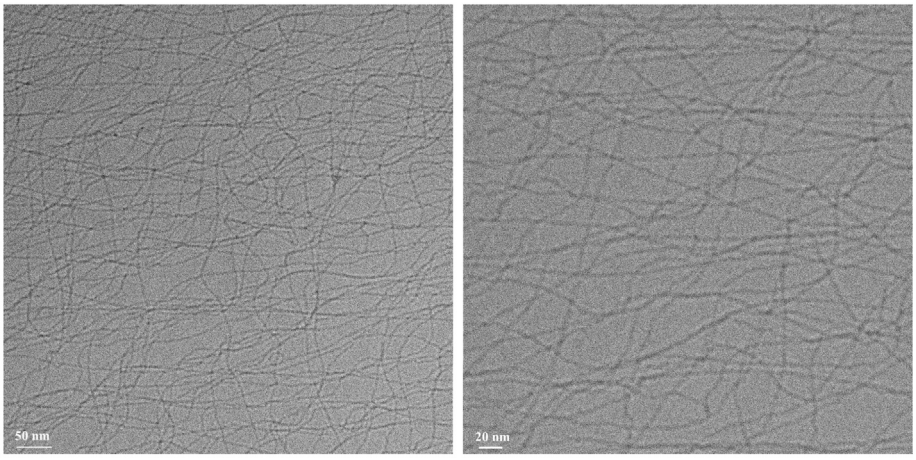

Fig. 2. Cryo-EM images of the CPyCl-Diclo micelles at 16.7 mMCpyCl 11.0 mM Diclo composition. The scale bar is displayed at the bottom left of each image.

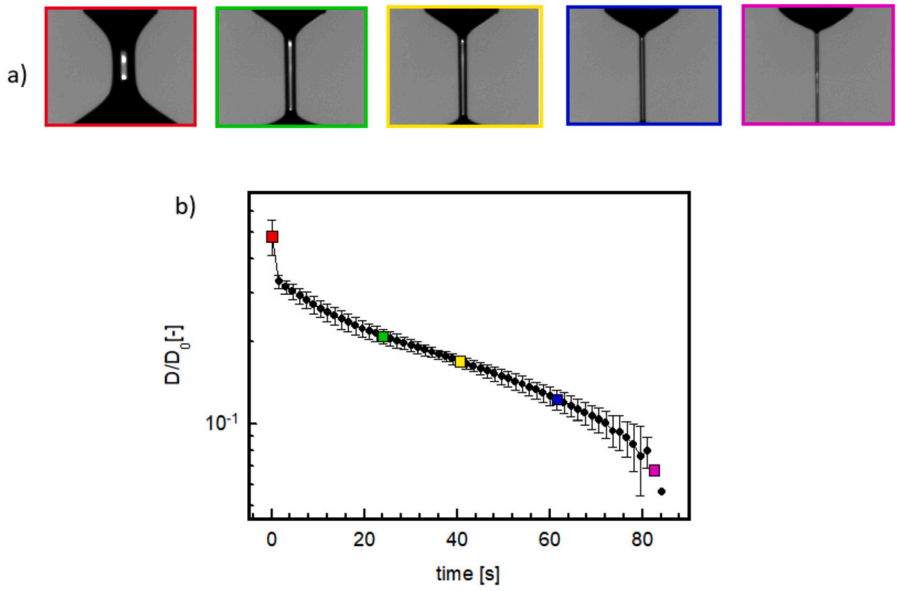

Fig. 3. Extensional test at $0.03s^{-1}$ on the micellar solution with the DoS setup. a) Snapshots during the experiment; b) Thinning diameter for the filament measured as a function of time. The colored squares refer to the time at which the snapshots are taken.

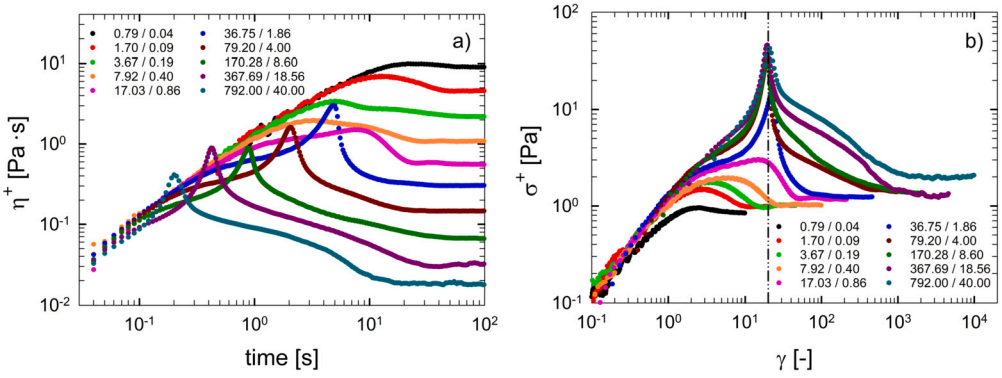

Fig. 4. a) The stress growth coefficient as a function of time and b) the shear stress growth function *vs* strain for the investigated solution at different applied shear rates. The legend reports two distinct Wi numbers: the first is obtained with the disengagement time, τ_d, while the second takes into account the breaking and reforming time, τ_b.

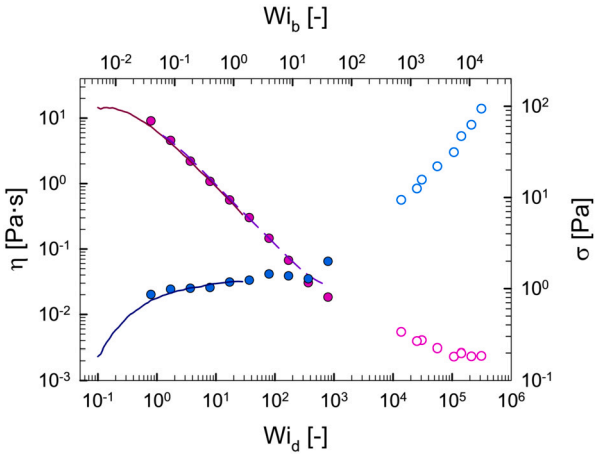

Fig. 5. Viscosity and shear stress flow curves of the investigated surfactant solution, acquired with both rotational and capillary rheometers. Full symbols are the steady state values obtained with start-up experiments. Empty symbols come from capillary measurements. The solid lines are continuous flow curves. The dashed line is the complex viscosity, obtained by applying the empirical Cox-Merz rule.

Here, N_{agg} is the number of surfactant molecules per micelle, obtained as the number of molecules in a single section per cylinder length unit [66] multiplied by the micelle contour length, reported in Table 1. φ is the volume fraction of the surfactant. The theoretical scission energy is equal to roughly 34 $k_BT \sim 1.4 \cdot 10^{-19}$ Joule. The two estimates agree surprisingly well but are significantly higher than the values reported in literature [40,67]. This is probably due to the high number of aggregation per single micelle and the low surfactant volume fraction, peculiar of this system. In SI, theoretical and experimental scission energy values have been evaluated for other systems, as a further proof of the possibility of applying this methodology [46,34].

3.2. WLMs flow curve

The viscosity steady state values at each shear rate can be plotted as a function of Wi_d (and Wi_b). To extend the range of Wi_d under investigation, we combined shear and capillary rheology measurements, as outlined in section 2. The lack of data in the Wi_d range between 10^3 and 10^4 arises from strong flow instabilities (in rotational rheology) and insufficient pressure (in capillary rheology).

Fig. 5 combines the flow curves as a function of Wi_d, the steady state values obtained with the start-up measurements, and the values at very high rates obtained with the capillary rheometry experiments. Shear stress shows a slight increase for $Wi_d<1$, after which a Wi-independent trend emerges, also found with the continuous flow curve (blue line), conventionally associated with a shear banding phenomenon [68]. The stress plateau lasts for more than two decades, after which a monotonic increase of the stress at Wi_d values higher than 400 is detected, as expected [36,67]. At very high deformation rates, indeed, the growth in the stress is again linear with respect to the shear rate, due to the presence and deformation of shorter micellar strands.

The viscosity of the micellar solution presents a shear thinning behavior in the whole investigated strain rate interval. The long worms align in the flow direction, stretch and break at very high shear rates [69]. For very high Wi_d values, the viscosity shows a secondary plateau value, very close to the viscosity value of the suspending medium, i.e. water. The specific viscosity, η_S, is reported in SI. At high Wi_d, η_S tends to unity, as a result of the massive WLMs breaking. This is in line with previous observations regarding shear banding suppression above a critical viscosity ratio [70].

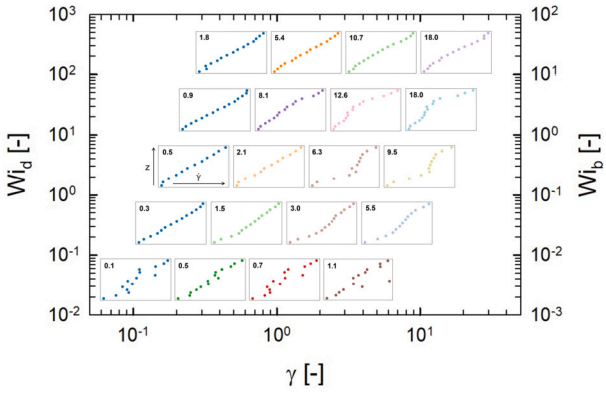

Fig. 6. Overview of the velocity profiles across the gap for different values of imposed shear rate and for different strain positions. Cumulated strain values are reported in the top left corner of each panel. Each inset plot shows the normalized strain value (x axis) at different positions along the gap (y axis). The values of the cumulated strain, Wi_d and Wi_b are also reported.

3.3. Rheo-microscopy

Previous neutron scattering experiments on viscoelastic WLMs reported the appearance of shear banding above a critical strain value [71], suggesting that a similar phenomenon may occur in our sample. This would also be consistent with the observed stress plateau in the flow curve. To assess this hypothesis in our system, we performed rheo-microscopy experiments, measuring the velocity of tracer particles at different heights in the gap and thus reconstructing flow profiles. Fig. 6 reports several of such profiles, for different imposed strain rates and for different times - or strains. Each inset plot shows the normalized strain value (x axis) at different positions along the gap (y axis). While at very low imposed shear rates all profiles are linear ($Wi_d<1$), corresponding to affine deformation, for larger shear rates ($Wi_d>1$) the profiles display the onset of shear banding for high enough cumulated strains. At even higher rates, banding seems to weaken. Unfortunately, the linear shear cell cannot cover the entire range of shear rates and strains accessible with a rotational rheometer. Nevertheless, it is apparent, also in this case, that the profiles show instability when Wi_d is roughly 1, and the deformation becomes significant, while they tend to approach again an affine behavior when reaching Wi_b. Of course, the comparison between the microscopic and the macroscopic responses cannot be fully quantitative, since the two geometries are different and the rheological response is, in any case, a picture of the “average” sample behavior.

4. Discussion and conclusions

An in-depth study was conducted on a selected solution of WLMs, combining several techniques, such as shear/extensional/capillary rheology, cryo-EM, and rheo-microscopy. Linear rheology allows to cover the entire relaxation spectrum of the sample, enabling the estimation of the main characteristic parameters and lengths. Micelles were found to be significantly long and poorly entangled, exhibiting a reptation time of the order of hundreds of seconds. This has also been confirmed through linear extensional rheology. Cryo-EM images proved the presence of extremely long micelles and of a loosely entangled network.

The nonlinear rheological response of these WLMs in start-up flow revealed two main phenomena: shear banding and strain hardening. These phenomena happen on completely different time scales. Shear banding appears much before any breaking event takes place, and the characteristic time for the onset of the banding transition is the total relaxation time. The transition from a homogeneous flow field to an inhomogeneous one characterized by the presence of two bands is confirmed through rheo-microscopy.

When the shear rate exceeds the inverse of the breaking and renewing process of the WLMs, these chains are somehow frozen and there is the experimental evidence of their finite extensibility. A rubber-like response is detected, with a catastrophic breakage phenomenon appearing at 20 strain units, above which the system totally collapses. When the system is disrupted and composed by smaller micelles and/or disconnected surfactant molecules in water the solution does not anymore band. By borrowing existing formulas from the rubber elasticity, it has been possible to experimentally evaluate the scission energy, which was found in very good agreement with the theoretical one.

This study sheds a light on the dynamics in fast flows of long and entangled wormlike surfactant solutions, being able to differentiate and decouple banding and breaking. The physical correlation, if any, between the two phenomena, as well as the reasons for the onset of the shear banding to occur, are still pending.

CRediT authorship contribution statement

Ilaria Cusano: Writing – original draft, Software, Methodology, Investigation, Formal analysis, Data curation. **Afshin Azarpour:** Writing – original draft, Software, Investigation, Data curation. **Luca Laugeni:** Writing – original draft, Software, Investigation. **Simona Russo Spena:** Writing – original draft, Software, Investigation. **Pedro Rodriguez Gonzalez:** Investigation, Formal analysis. **Dganit Danino:** Writing – review & editing, Validation, Funding acquisition. **Nino Grizzuti:** Writing – review & editing, Supervision, Project administration, Funding acquisition. **Giuliano Zanchetta:** Writing – review & editing, Project administration, Funding acquisition, Data curation, Conceptualization. **Rossana Pasquino:** Writing – original draft, Supervision, Resources, Project administration, Funding acquisition, Formal analysis, Data curation, Conceptualization.

Declaration of competing interest

The authors declare that they have no known competing financial interests or personal relationships that could have appeared to influence the work reported in this paper.

Acknowledgements

Francesco Greco is fully acknowledged for fruitful discussions. RP acknowledges TA Instruments for awarding the DHR rheometer used in this study as part of the Distinguished Young Rheologist Award 2018.

Appendix A. Supplementary material

Supplementary material related to this article can be found online at https://doi.org/10.1016/j.jcis.2025.137725.

Data availability

Data will be made available on request.

References

[1] J. Yang, Viscoelastic wormlike micelles and their applications, Curr. Opin. Colloid Interface Sci. 7 (5) (2002) 276–281, https://doi.org/10.1016/S1359-0294(02)00071-7.
[2] Z. Chu, C.A. Dreiss, Y. Feng, Smart wormlike micelles, Chem. Soc. Rev. 42 (2013) 7174–7203, https://doi.org/10.1039/C3CS35490C.
[3] H. Rehage, H. Hoffmann, Rheological properties of viscoelastic surfactant systems, J. Phys. Chem. 92 (16) (1988) 4712–4719, https://doi.org/10.1021/j100327a031.
[4] R.G. Larson, The Structure and Rheology of Complex Fluids, Oxford University Press, Inc., 1999.
[5] H. Hoffmann, G. Ebert, Surfactants, micelles and fascinating phenomena, Angew. Chem., Int. Ed. Engl. 27 (7) (1988) 902–912, https://doi.org/10.1002/anie.198809021.
[6] Z. Lin, J.J. Cai, L.E. Scriven, H.T. Davis, Spherical-to-wormlike micelle transition in ctab solutions, J. Phys. Chem. 98 (23) (1994) 5984–5993, https://doi.org/10.1021/j100074a027.
[7] T.H. Ito, P.C.M.L. Miranda, N.H. Morgon, G. Heerdt, C.A. Dreiss, E. Sabadini, Molecular variations in aromatic cosolutes: critical role in the rheology of cationic wormlike micelles, Langmuir 30 (39) (2014) 11535–11542, https://doi.org/10.1021/la502649j.
[8] P. Venkatesan, Y. Cheng, D. Kahne, Hydrogen bonding in micelle formation, J. Am. Chem. Soc. 116 (15) (1994) 6955–6956, https://doi.org/10.1021/ja00094a068.
[9] H. Rehage, H. Hoffmann, Viscoelastic surfactant solutions: model systems for rheological research, Mol. Phys. 74 (5) (1991) 933–973, https://doi.org/10.1080/00268979100102721.
[10] C.A. Dreiss, Wormlike micelles: where do we stand? Recent developments, linear rheology and scattering techniques, Soft Matter 3 (2007) 956–970, https://doi.org/10.1039/B705775J.
[11] N. Vlachy, M. Drechsler, J.-M. Verbavatz, D. Touraud, W. Kunz, Role of the surfactant headgroup on the counterion specificity in the micelle-to-vesicle transition through salt addition, J. Colloid Interface Sci. 319 (2) (2008) 542–548, https://doi.org/10.1016/j.jcis.2007.11.048.
[12] M.E. Cates, S.J. Candau, Statics and dynamics of worm-like surfactant micelles, J. Phys. Condens. Matter 2 (33) (1990) 6869, https://doi.org/10.1088/0953-8984/2/33/001.
[13] I. Cusano, I. Ionita, P.R. Gonzalez, D. Danino, N. Grizzuti, R. Pasquino, Drug-induced transitions from micelles to vesicles in ionic surfactant solutions, Colloids Surf. A, Physicochem. Eng. Asp. 690 (2024) 133793, https://doi.org/10.1016/j.colsurfa.2024.133793.
[14] M.E. Cates, Reptation of living polymers: dynamics of entangled polymers in the presence of reversible chain-scission reactions, Macromolecules 20 (9) (1987) 2289–2296, https://doi.org/10.1021/ma00175a038.
[15] R. Granek, M.E. Cates, Stress relaxation in living polymers: results from a Poisson renewal model, J. Chem. Phys. 96 (6) (1992) 4758–4767, https://doi.org/10.1063/1.462787.
[16] M. Rubinstein, R.H. Colby, Polymer Physics, Oxford University Press, 2003.
[17] C. Oelschlaeger, M. Schopferer, F. Scheffold, N. Willenbacher, Linear-to-branched micelles transition: a rheometry and diffusing wave spectroscopy (dws) study, Langmuir 25 (2) (2009) 716–723, https://doi.org/10.1021/la802323x.
[18] H. von Berlepsch, L. Harnau, P. Reineker, Persistence length of wormlike micelles from dynamic light scattering, J. Phys. Chem. B 102 (39) (1998) 7518–7522, https://doi.org/10.1021/jp980677x.
[19] J. Marignan, J. Appell, P. Bassereau, G. Porte, R.P. May, Local structures of the surfactant aggregates in dilute solutions deduced from small angle neutron scattering patterns, J. Phys. France 50 (24) (1989) 3553–3566, https://doi.org/10.1051/jphys:0198900500240355300.
[20] F. Lequeux, Reptation of connected wormlike micelles, Europhys. Lett. 19 (8) (1992) 675, https://doi.org/10.1209/0295-5075/19/8/003.
[21] W. Zou, R.G. Larson, A mesoscopic simulation method for predicting the rheology of semi-dilute wormlike micellar solutions, J. Rheol. 58 (3) (2014) 681–721, https://doi.org/10.1122/1.4868875.
[22] J.D. Peterson, W. Zou, R.G. Larson, M.E. Cates, Wormlike micelles revisited: a comparison of models for linear rheology, J. Non-Newton. Fluid Mech. 322 (2023) 105149, https://doi.org/10.1016/j.jnnfm.2023.105149.
[23] W. Zou, G. Tan, M. Weaver, P. Koenig, R.G. Larson, Mesoscopic modeling of the effect of branching on the viscoelasticity of entangled wormlike micellar solutions, Phys. Rev. Res. 5 (2023) 043024, https://doi.org/10.1103/PhysRevResearch.5.043024.
[24] G. Tan, R.G. Larson, Quantitative modeling of threadlike micellar solution rheology, Rheol. Acta 61 (7) (2022) 443–457, https://doi.org/10.1007/s00397-022-01341-4.
[25] W. Zou, G. Tan, H. Jiang, K. Vogtt, M. Weaver, P. Koenig, G. Beaucage, R.G. Larson, From well-entangled to partially-entangled wormlike micelles, Soft Matter 15 (2019) 642–655, https://doi.org/10.1039/C8SM02223B.
[26] G. Tan, W. Zou, M. Weaver, R.G. Larson, Determining threadlike micelle lengths from rheometry, J. Rheol. 65 (1) (2020) 59–71, https://doi.org/10.1122/8.0000152.
[27] E. Kesselman, D. Danino, Direct-imaging cryo-transmission electron microscopy of wormlike micelles, in: Wormlike Micelles: Advances in Systems, Characterisation and Applications, The Royal Society of Chemistry, 2017.
[28] D. Danino, T. Zemb, On the shape and connections of micelles: electron microscopy imaging inspiring thermodynamic modelling, Curr. Opin. Colloid Interface Sci. 61 (2022) 101607, https://doi.org/10.1016/j.cocis.2022.101607.
[29] L. Abezgauz, K. Kuperkar, P.A. Hassan, O. Ramon, P. Bahadur, D. Danino, Effect of hofmeister anions on micellization and micellar growth of the surfactant cetylpyridinium chloride, J. Colloid Interface Sci. 342 (2010) 83–92, https://doi.org/10.1016/j.jcis.2009.08.045.
[30] T. Shikata, H. Hirata, E. Takatori, K. Osaki, Nonlinear viscoelastic behavior of aqueous detergent solutions, J. Non-Newton. Fluid Mech. 28 (2) (1988) 171–182, https://doi.org/10.1016/0377-0257(88)85038-9.
[31] J. Berret, D.C. Roux, Rheology of nematic wormlike micelles, J. Rheol. 39 (4) (1995) 725–741, https://doi.org/10.1122/1.550654.
[32] J.-F. Berret, Transient rheology of wormlike micelles, Langmuir 13 (8) (1997) 2227–2234, https://doi.org/10.1021/la961078p.
[33] P.D. Olmsted, Perspectives on shear banding in complex fluids, Rheol. Acta 47 (3) (2008) 283–300, https://doi.org/10.1007/s00397-008-0260-9.

[34] T. Inoue, Y. Inoue, H. Watanabe, Nonlinear rheology of ctab/nasal aqueous solutions: finite extensibility of a network of wormlike micelles, Langmuir 21 (4) (2005) 1201–1208, https://doi.org/10.1021/la048292v.
[35] S. Varchanis, S.J. Haward, C.C. Hopkins, J. Tsamopoulos, A.Q. Shen, Evaluation of constitutive models for shear-banding wormlike micellar solutions in simple and complex flows, J. Non-Newton. Fluid Mech. 307 (2022) 104855, https://doi.org/10.1016/j.jnnfm.2022.104855.
[36] R.L. Moorcroft, S.M. Fielding, Shear banding in time-dependent flows of polymers and wormlike micelles, J. Rheol. 58 (1) (2014) 103–147, https://doi.org/10.1122/1.4842155.
[37] J.-B. Salmon, A. Colin, S. Manneville, F.m.c. Molino, Velocity profiles in shear-banding wormlike micelles, Phys. Rev. Lett. 90 (2003) 228303, https://doi.org/10.1103/PhysRevLett.90.228303, https://link.aps.org/doi/10.1103/PhysRevLett.90.228303.
[38] E.F. Brown, W.R. Burghardt, D.C. Venerus, Tests of the lodge Meissner relation in anomalous nonlinear step strain of an entangled wormlike micelle solution, Langmuir 13 (1997) 3902–3904, https://doi.org/10.1021/la9700376.
[39] R.K. Prud'homme, G.G. Warr, Elongational flow of solutions of rodlike micelles, Langmuir 10 (10) (1994) 3419–3426, https://doi.org/10.1021/la00022a010.
[40] J.P. Rothstein, Transient extensional rheology of wormlike micelle solutions, J. Rheol. 47 (5) (2003) 1227–1247, https://doi.org/10.1122/1.1603242.
[41] M.S. Turner, M.E. Cates, Flow-induced phase transitions in rod-like micelles, J. Phys. Condens. Matter 4 (14) (1992) 3719, https://doi.org/10.1088/0953-8984/4/14/005.
[42] A. Bhardwaj, D. Richter, M. Chellamuthu, J.P. Rothstein, The effect of pre-shear on the extensional rheology of wormlike micelle solutions, Rheol. Acta 46 (6) (2007) 861–875, https://doi.org/10.1007/s00397-007-0168-9.
[43] S. Majumdar, A.K. Sood, Nonlinear viscoelasticity of entangled wormlike micellar fluid under large-amplitude oscillatory shear: role of elastic Taylor-Couette instability, Phys. Rev. E 89 (2014), https://doi.org/10.1103/PhysRevE.89.062314.
[44] D. Sachsenheimer, B. Hochstein, N. Willenbacher, Experimental study on the capillary thinning of entangled polymer solutions, Rheol. Acta 53 (9) (2014) 725–739, https://doi.org/10.1007/s00397-014-0789-8.
[45] S. Fujii, H. Morikawa, M. Ito, T. Takahashi, Transient behavior of stress in a wormlike micellar solution under oscillatory shear, Colloid Polym. Sci. 293 (11) (2015) 3237–3248, https://doi.org/10.1007/s00396-015-3674-9.
[46] R. Pasquino, P.R. Avallone, S. Costanzo, I. Inbal, D. Danino, V. Ianniello, G. Ianniruberto, G. Marrucci, N. Grizzuti, On the startup behavior of wormlike micellar networks: the effect of different salts bound to the same surfactant molecule, J. Rheol. 67 (2) (2023) 353–364, https://doi.org/10.1122/8.0000537.
[47] V. Vitali, G. Nava, G. Zanchetta, F. Bragheri, A. Crespi, R. Osellame, T. Bellini, I. Cristiani, P. Minzioni, Integrated optofluidic chip for oscillatory microrheology, Sci. Rep. 10 (1) (2020) 5831, https://doi.org/10.1038/s41598-020-62628-1.
[48] V. Vitali, G. Nava, A. Corno, M. Pezzotti, F. Bragheri, P. Paiè, R. Osellame, M.A. Ortenzi, I. Cristiani, P. Minzioni, T. Bellini, G. Zanchetta, Yield stress "in a flash": investigation of nonlinearity and yielding in soft materials with an optofluidic microrheometer, Soft Matter 17 (2021) 3105–3112, https://doi.org/10.1039/D0SM02168G.
[49] A.K. Gurnon, C.R. Lopez-Barron, A.P.R. Eberle, L. Porcar, N.J. Wagner, Spatiotemporal stress and structure evolution in dynamically sheared polymer-like micellar solutions, Soft Matter 10 (2014) 2889–2898, https://doi.org/10.1039/C3SM53113A.
[50] P. Edera, M. Brizioli, G. Zanchetta, G. Petekidis, F. Giavazzi, R. Cerbino, Deformation profiles and microscopic dynamics of complex fluids during oscillatory shear experiments, Soft Matter 17 (2021) 8553–8566, https://doi.org/10.1039/D1SM01068A.
[51] G. Zanchetta, E. Rocchi, L. Piazza, Seeing is believing: coupling between liquid crystalline ordering and rheological behaviour in cellulose nanocrystals suspensions, Chem. Eng. Trans. 57 (2017) 1933–1938, https://doi.org/10.3303/CET1757323.
[52] S. Villa, P. Edera, M. Brizioli, V. Trappe, F. Giavazzi, R. Cerbino, Quantitative rheo-microscopy of soft matter, Front. Phys. 10 (2022), https://doi.org/10.3389/fphy.2022.1013805, https://www.frontiersin.org/journals/physics/articles/10.3389/fphy.2022.1013805.
[53] R.H. Ewoldt, M.T. Johnston, L.M. Caretta, Experimental Challenges of Shear Rheology: How to Avoid Bad Data, Springer New York, New York, NY, 2015, pp. 207–241.
[54] S. Russo Spena, B. Visone, N. Grizzuti, An engineering approach to the 3d printing of k-carrageenan/konjac glucomannan hydrogels, Int. J. Food Sci. Technol. 59 (6) (2024) 4122–4133, https://doi.org/10.1111/ijfs.17170.
[55] C.W. Macosko, Rheology: Principles, Measurements, and Applications, Wiley - VCH Publishers, New York, 1994.
[56] D.Y. Zhang, M.A. Calabrese, Temperature-controlled dripping-onto-substrate (dos) extensional rheometry of polymer micelle solutions, Soft Matter 18 (2022) 3993–4008, https://doi.org/10.1039/D2SM00377E.
[57] K.T. Lauser, A.L. Rueter, M.A. Calabrese, Small-volume extensional rheology of concentrated protein and protein-excipient solutions, Soft Matter 17 (2021) 9624–9635, https://doi.org/10.1039/D1SM01253C.
[58] J.-B. Boitte, C. Vizcaïno, L. Benyahia, J.-M. Herry, C. Michon, M. Hayert, A novel rheo-optical device for studying complex fluids in a double shear plate geometry, Rev. Sci. Instrum. 84 (1) (2013), https://doi.org/10.1063/1.4774395.
[59] D. Danino, Cryo-tem of soft molecular assemblies, Curr. Opin. Colloid Interface Sci. 17 (6) (2012) 316–329, https://doi.org/10.1016/j.cocis.2012.10.003.
[60] V. Calabrese, A.Q. Shen, S.J. Haward, How do polymers stretch in capillary-driven extensional flows?, Macromolecules (2024), https://doi.org/10.1021/acs.macromol.4c01604.
[61] A. Gaillard, M.A. Herrada, A. Deblais, J. Eggers, D. Bonn, Beware of caber: filament thinning rheometry does not always give 'the' relaxation time of polymer solutions, Phys. Rev. Fluids 9 (2024) 073302, https://doi.org/10.1103/PhysRevFluids.9.073302.
[62] D.Y. Zhang, M.A. Calabrese, Temperature-controlled dripping-onto-substrate (dos) extensional rheometry of polymer micelle solutions, Soft Matter 18 (2022) 3993–4008, https://doi.org/10.1039/D2SM00377E.
[63] D. Gaudino, S. Costanzo, G. Ianniruberto, N. Grizzuti, R. Pasquino, Linear wormlike micelles behave similarly to entangled linear polymers in fast shear flows, J. Rheol. 64 (4) (2020) 879–888, https://doi.org/10.1122/8.0000003.
[64] B. Wen, B. Bai, R.G. Larson, Surfactant desorption and scission free energies for cylindrical and spherical micelles from umbrella-sampling molecular dynamics simulations, J. Colloid Interface Sci. 599 (2021) 773–784, https://doi.org/10.1016/j.jcis.2021.04.138.
[65] E. Lifshitz, A. Kosevich, L. Pitaevskii, Chapter I - fundamental equations, in: Theory of Elasticity, third edition, Butterworth-Heinemann, Oxford, 1986, pp. 1–37.
[66] T. Shikata, S.J. Dahman, D.S. Pearson, Rheo-optical behavior of wormlike micelles, Langmuir 10 (10) (1994) 3470–3476, https://doi.org/10.1021/la00022a019.
[67] P.A. Vasquez, G.H. McKinley, L. Pamela Cook, A network scission model for wormlike micellar solutions: I. Model formulation and viscometric flow predictions, J. Non-Newton. Fluid Mech. 144 (2) (2007) 122–139, https://doi.org/10.1016/j.jnnfm.2007.03.007.
[68] E. Miller, J.P. Rothstein, Transient evolution of shear-banding wormlike micellar solutions, J. Non-Newton. Fluid Mech. 143 (1) (2007) 22–37, https://doi.org/10.1016/j.jnnfm.2006.12.005.
[69] J.-F. Berret, Rheology of Wormlike Micelles: Equilibrium Properties and Shear Banding Transitions, Springer Netherlands, 2006, pp. 667–720.
[70] T. Divoux, M.A. Fardin, S. Manneville, S. Lerouge, Shear banding of complex fluids, Annu. Rev. Fluid Mech. 48 (2016) 81–103, https://doi.org/10.1146/annurev-fluid-122414-034416.
[71] S.A. Rogers, M.A. Calabrese, N.J. Wagner, Rheology of branched wormlike micelles, Curr. Opin. Colloid Interface Sci. 19 (6) (2014) 530–535, https://doi.org/10.1016/j.cocis.2014.10.006.